

# Modeling Air Entrainment and Temperature Effects in Winding

H. Lei

e-mail: herong.lei@Kodak.com

K. A. Cole

S. J. Weinstein

Eastman Kodak Company,  
Rochester, NY 14652

*Rolls of films and paper are routinely stored under varying conditions before being unwound into downstream operations. During storage, interlayer pressures can change relative to the pressures generated during winding. These changes can lead to problems such as film/paper blocking (increased interlayer pressure) and roll shifting/cinching (decreased interlayer pressure). To study the storage effect, a nonlinear wound roll stress model including air entrainment is first developed and applied to predict the in-roll stresses during film/paper winding. Thereafter, a thermal stress model is used to study the temperature effect on wound roll stresses. Key inputs to the models are the stack modulus, contact clearance, and air film reference clearance. A method is developed to measure these key model inputs. Results of a parametric study show that among the processing conditions, storage temperature and thermal expansion coefficients of the core and the film/paper are key factors that affect in-roll stresses during storage. Limitations of the models will also be discussed along with recommendations for future modeling development. [DOI: 10.1115/1.1629758]*

## 1 Introduction

Wound roll quality is primarily a function of the level and distribution of stresses developed within a roll both during and after winding. Because of this relationship, developing an improved understanding of wound roll stresses has historically been the main driver in the development of wound roll models. It is well known that wound roll stresses are influenced by many factors including process parameters, product parameters, and environmental conditions. Owing to the increasing desire to streamline process and product design, the complexity of wound roll models has increased over the last few years. In particular, researchers have sought to include more of the factors influencing wound roll stresses into the models. The wound roll model presented in this paper seeks to combine physical effects that have been studied in the past. In addition, a discussion is presented noting the limitations of the model along with recommendations for future modeling.

There is a rich history of literature devoted to the wound roll problem. We will cite only a few selected papers here. One of the earliest works was that of Altmann [1] who idealized the winding process as the addition of a sequence of stretched hoops shrink fit onto the roll. This idealization has been employed ever since. He further assumed that the roll could be modeled as a linear orthotropic material enabling an analytic solution to the winding problem. Connolly and Winarski [2] built on Altmann's work by adding temperature and humidity effects. They formulated the problem in terms of radial displacements and obtained solutions numerically. Hakiel [3] extended the earlier works by treating the roll as a nonlinear orthotropic material, specifically noting that the radial compressive modulus is a nonlinear function of pressure. Solutions were obtained numerically using a quasilinearization procedure. Qualls [4] extended the work of Hakiel [3] by including the thermoelastic effect into the winding model. The problem was formulated in terms of radial stress and verification experiments were presented. Results indicated that the thermoelastic behavior could have a significant impact on wound roll stress level.

Good et al. [5] further extended Hakiel's formulation to include the effect of an idling pressure roll (Fig. 1). Pressure rolling is used to minimize air entrainment and Good showed that, at low winding speeds, a simple modification to the outer lap pressure boundary condition is required to model the effect. Good and Holmberg [6] were the first to add air entrainment to the centerwinding model. Foil bearing theory was used to estimate the amount of entrained air while the in-roll problem was treated by modifying the Hakiel formulation to include an additional component of radial compressive modulus because of isothermal compression of air. Side leakage was not considered in their formulation. Good and Covell [7] examined air entrainment in the presence of an idling pressure roll. A simple hydrodynamic model without compressibility was used to estimate the magnitude of entrained air. The in-roll problem was treated as in Good and Holmberg [6]. A more detailed theoretical study of air entrainment in the presence of a nip roller was performed by Chang et al. [8] This work showed that air compressibility has a significant impact on the amount of air that passes through the nip. An experimental study was performed by Taylor and Good [9] which showed that Chang's work accurately predicts the magnitude of entrained air.

Forrest [10,11] formulated a more complete air entrainment centerwinding model by considering roughness and air pressure coupling under the idling pressure roll. The in-roll problem was solved using a plane-strain formulation. A buckling analysis was also presented enabling prediction of machine and cross direction buckles. Bouquerel and Bourgin [12] presented a similar model, but like Good and Covell [7], they used an air entrainment nip model that neglected contact between the pressure roll and the winding roll. One extension that was considered in the model was an empirical treatment of side leakage during and after winding. Later papers, i.e., Bourgin [13] and Forrest [14], surveyed the state of art in winding models and included in their discussions air entrainment, side leakage, and wound roll defect prediction. It was noted that the time scale of side leakage was highly dependent on factors such as initial lap-to-lap clearance and web width. Finally, several papers, Pfeiffer [15,16] and Forrest [17], provided discussions and work directed toward the measurement of the radial compressive modulus. It is clear from these references that the measurement of this property requires care. Details such as sample preparation, test equipment, test procedures, and data analysis can all have a major impact on experimental results.

The main objective of the present study is to present a model that combines the effects of air entrainment during pressure roll centerwinding with the thermoelastic effect after winding. Meth-

Contributed by the Applied Mechanics Division of THE AMERICAN SOCIETY OF MECHANICAL ENGINEERS for publication in the ASME JOURNAL OF APPLIED MECHANICS. Manuscript received by the ASME Applied Mechanics Division, October 15, 2002; final revision, June 4, 2003. Associate Editor: R. C. Benson. Discussion on the paper should be addressed to the Editor, Prof. Robert M. McMeeking, Department of Mechanical and Environmental Engineering University of California—Santa Barbara, Santa Barbara, CA 93106-5070, and will be accepted until four months after final publication of the paper itself in the ASME JOURNAL OF APPLIED MECHANICS.

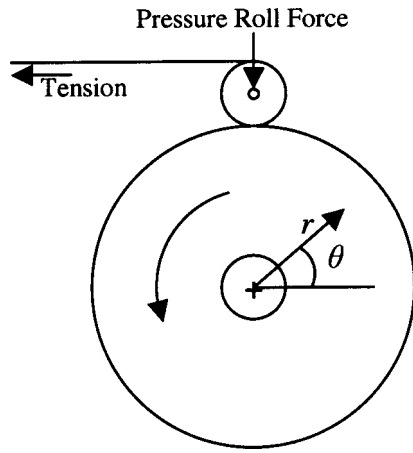


Fig. 1 Center winding with an idling pressure roll. Center of the winding roll is driven by a motor.

ods to measure the inputs to the model are discussed. Experimental results validating the winding model are also presented. A parametric study is presented that indicates the mitigating effect of air entrainment on the impact of thermoelastic expansion on wound roll stresses. It is finally noted that side leakage is not considered in the model. A detailed analysis is presented justifying this approach. This analysis provides quantitative guidance as to when side leakage must be considered and further provides insight into future model extensions.

## 2 Air Entrainment Winding Model

In this section, the air entrainment winding model is developed. First, a model for web roughness is presented. This model, along with the theoretical results from Chang et al. [8] is then used to analyze the amount of air entrained into the wound roll as the web passes between the pressure roll and the winding roll. Finally, the in-roll model is derived and includes the combined effects of roughness contact and air pressure.

**2.1 Web Roughness Model.** In order to determine the amount of air entrainment during winding, a simple model for web roughness is first presented. The roughness parameters used in the air entrainment model are defined in Fig. 2. Part (a) of the figure shows a cross section of two webs at incipient contact in vacuum conditions. As compressive loading is applied to the webs, displacements will occur in the roughness interface and within the support. The contact reference clearance,  $cc_o$ , is defined as the combined height of the roughness over which interfacial displacements occur. The air film reference clearance,  $ca_o$ , is the average of void space (gap) between two webs at the incipient contact condition. Contact and air film reference clearances are determined from Wyko® surface roughness measurements of both the front and backside of the web. Two of the key parameters from the Wyko® measurements are the peak-to-valley surface roughness  $R_z$  and mean-peak-roughness,  $R_{pm}$ . In the model, the root-mean-square of the front and backside  $R_z$  are used as the contact reference clearance,  $cc_o$ . The root-mean-square of the engagement heights of the front and back surfaces, [18], is used as an approximation to the air film reference clearance,  $ca_o$ .

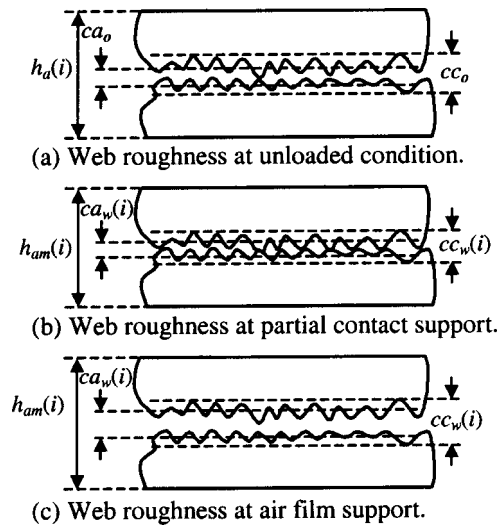


Fig. 2 Web roughness model

Part (b) and (c) in Fig. 2 show the geometry for two cases that are possible once air entrainment occurs. Part (b) shows the corresponding contact clearance,  $cc_w(i)$ , and air film clearance,  $ca_w(i)$ , under the outer lap away from the web/pressure roller nip for winding conditions where roughness contact occurs. The variable  $i$  indicates the lap number. Note that the clearance,  $cc_w(i)$ , between two webs is reduced relative to the contact reference clearance,  $cc_o$ . This will occur under low speed winding where the air entrainment effect is minimal. On the other hand, for high-speed winding when the pressure roller load is not sufficiently large, the air film clearance will be increased from the reference clearance as the outer lap winds onto the roll because of air entrainment (Part (c)). In this case all the belt wrap loading will be air supported.

In addition to the clearance definitions under the outer lap, the contact clearance,  $cc(i)$ , and the air film clearance,  $ca(i)$ , within the wound roll are also defined. These additional variables are needed to enable the model to track clearance and interlayer pressure as the roll winds.

**2.2 Pressure Roller Nip Analysis.** From the above discussion, it is clear that for a nonzero winding speed under nonvacuum conditions, air will always contribute to the interlayer pressure. In order to determine the magnitude of this contribution during pressure roller winding, the air entrained in the outer lap must first be determined.

Consider a winding roll with widthwise invariant web and core properties. Under the pressure roller, the nip force per web width,  $f_p(i)$ , is comprised of an air force,  $f_a(i)$ , and/or a contact force,  $f_c(i)$ :

$$f_p(i) = f_a(i) + f_c(i). \quad (1)$$

The air force arises because of entraining of air and the contact force arises if the web wrapping the pressure roller is in physical contact to the roll through its rough surface. From Chang et al. [8], the air film clearance beneath the pressure roller nip,  $ca_n(i)$ , can be expressed as a function of the developed air force  $f_a(i)$ :

$$\frac{ca_n(i)}{R(i)} = \begin{cases} 6.5 \left( \frac{\mu V}{p_a R(i)} \right)^{0.65} \left( \frac{f_a(i)}{p_a R(i)} \right)^{-0.28} \left( \frac{E(i)}{p_a} \right)^{-0.44} & \text{for } 0.69 \leq E \leq 4.84 \text{ MPa} \\ 8.7 \left( \frac{\mu V}{p_a R(i)} \right)^{0.72} \left( \frac{f_a(i)}{p_a R(i)} \right)^{-0.49} \left( \frac{E(i)}{p_a} \right)^{-0.48} & \text{for } 4.84 \leq E \leq 34.5 \text{ MPa} \end{cases} \quad (2)$$

where  $V$  is the winding speed,  $p_a$  is atmospheric pressure, and  $R(i)$  and  $E(i)$  are the equivalent radius and equivalent modulus of the pressure roller/winding roll.

The air film clearance is related to the contact clearance if it is assumed that under loading, the reduction in contact clearance is equivalent to the reduction in air clearance:

$$cc_n(i) - cc_o = ca_n(i) - ca_o. \quad (3)$$

This assumption is not rigorously justified; however for typical loads and for webs dominated by very fine roughness with a random distribution of sparse high roughness, this would seem to be a reasonable assumption since the interfacial displacements would occur mainly in these high roughness areas.

From the Hertzian contact theory, [19], the contact force,  $f_c(i)$ , in terms of the contact clearance,  $cc_n(i)$ , is found to be

$$f_c(i) = \frac{\pi R(i)}{E(i)} P_n^2(cc_n(i)), \quad (4)$$

where  $P_n(cc_n)$  is the contact pressure under the nip and is related to the contact clearance via a look up table generated from the stack modulus measurement:

$$P_n(cc_n(i)) = f(cc_n(i)) = \begin{cases} f^*(cc_n(i)) & \text{for } cc_n \leq cc_o \\ 0 & \text{for } cc_n > cc_o \end{cases} \quad (5)$$

The above equations are well posed to solve for the unknowns under the nip,  $cc_n(i)$ ,  $ca_n(i)$ ,  $f_c(i)$ , and  $f_a(i)$ .

**2.3 Internal Outer Lap Analysis.** The analysis of this section uses the results of the pressure roller nip analysis to determine the air film clearance, air pressure, and contact condition under the outer lap away from the nip.

Empirical studies, [7], have shown that the effective winding tension (wound-in-tension) in pressure roller winding,  $t_a(i)$ , can be expressed as

$$t_a(i) = t(i) + \mu_w w f_c(i), \quad (6)$$

where  $\mu_w$  is the front-to-back friction coefficient of the web,  $w$  is the width of the web and  $t(i)$  is the upstream winding tension. This expression indicates that an additional component, known as the nip-induced tension, arises during winding when a pressure roller is added.

The winding tension stress under the outer lap away from the nip is related to the effective winding tension by

$$\frac{ca_a(i)}{R(i)} = \begin{cases} 7.4 \left( \frac{\mu V}{p_a R(i)} \right)^{0.66} \left( \frac{f_a(i)}{p_a R(i)} \right)^{-0.21} \left( \frac{E(i)}{p_a} \right)^{-0.33} & \text{for } 0.69 \leq E \leq 4.84 \text{ MPa} \\ 12.5 \left( \frac{\mu V}{p_a R(i)} \right)^{0.71} \left( \frac{f_a(i)}{p_a R(i)} \right)^{-0.20} \left( \frac{E(i)}{p_a} \right)^{-0.23} & \text{for } 4.84 \leq E \leq 34.5 \text{ MPa} \end{cases}, \quad (9)$$

where  $ca_a(i)$  is the air film clearance under the outer lap away from the nip adjusted to atmospheric pressure. The second relates the air pressure to the air film clearance using the perfect gas law:

$$p_a ca_a(i) = (p_a + P'_g(i)) ca_w(i). \quad (10)$$

By using the relation between  $ca_w(i)$  and  $cc_w(i)$  (the same fashion as in Eq. (3)), the above becomes

$$P'_g(i) = \frac{p_a ca_a(i)}{cc_w(i) - cc_o + ca_o} - p_a. \quad (11)$$

Once the pressure roller air load is determined, the above equations can be solved for contact clearance and air pressure under the outer lap away from the nip.

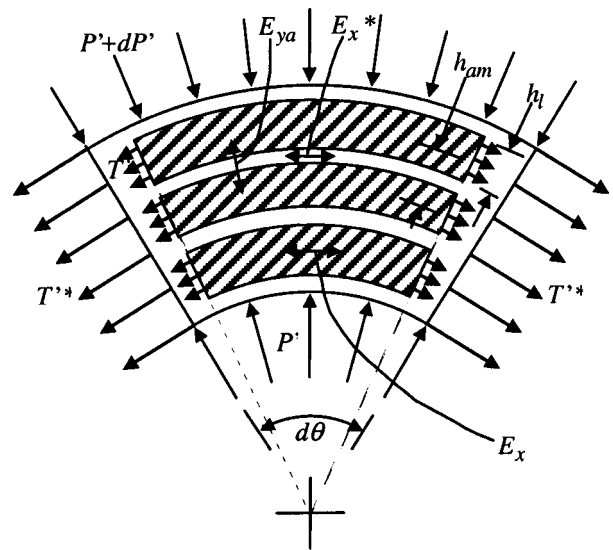


Fig. 3 Continuum differential force element in the wound roll

$$\sigma_\theta(i) = \frac{t_a(i)}{wh_l}, \quad (7)$$

where  $h_l$  is the load sharing web thickness (Fig. 3). The belt wrap pressure under the outer lap away from the nip is supported by air pressure and possibly contact pressure:

$$P'(i) = \frac{h_l \sigma_\theta(i)}{r_d(i)} = \frac{t_a(i)}{w r_d(i)} = P'_g(i) + P'_c(i). \quad (8)$$

The contact pressure is related to the contact clearance in the same fashion as Eq. (5). The air pressure under the outer lap away from the nip,  $P'_g(i)$ , is related to the air film clearance by a sequence of two equations. The first, according to Chang et al. [8], relates the clearance adjusted to atmospheric pressure to the pressure roller air load,  $f_a(i)$ ,

**2.4 In-Roll Analysis.** Prior to the addition of the next lap, say the  $i$ th, the roll will have a radius,  $r_d(i)$ . Assume that the next lap under wound-in-tension,  $t_a(i)$ , is added to the roll. The roll profile after the addition of the  $i$ th lap,  $r_d(i+1)$  is

$$r_d(i+1) = r_d(i) + U'(i) + h_{am}(i), \quad (12)$$

where  $U'(i)$  is the radial displacement of the roll due to the force exerted by the  $i$ th lap and  $h_{am}(i)$  is the reference web thickness added to the roll profile accounting for air entrainment and contact if present

$$h_{am}(i) = h_a + cc_w(i) - cc_o. \quad (13)$$

The derivation of in-roll analysis begins by considering the forces that act on a differential element located in the wound roll at a nominal wound roll radius. Figure 3 shows such an element that can be thought of as a continuum equivalent of the actual situation where the load sharing web thickness,  $h_l$ , will be less than the reference web thickness,  $h_{am}(i)$ .

To accommodate this difference, two in-roll tension stress parameters are defined. The first,  $T'^*$ , is the continuum approximation to the actual incremental in-roll stress,  $T'$ , which is distributed over the load sharing thickness. The apostrophe is added to denote that the stresses are incremental due to the addition of a single lap. In addition, anisotropic constitutive properties are defined for the continuum approximation ( $E_x^*$ ,  $\nu_{r\theta}^*$ , and  $\nu_{\theta r}^*$ ).

To simplify the development of the remaining equations in this section, explicit reference to lap number will be excluded from the model variables. It is understood that the stresses are evaluated at each lap.

Consider first the continuum approximation. A fundamental relationship between the continuum in-roll tension stress,  $T'^*$ , and the interlayer pressure stress,  $P'$ , can be obtained by force equilibrium:

$$P' + T'^* + r \frac{dP'}{dr} = 0. \quad (14)$$

The continuum in-roll tension stress is related to the actual in-roll tension stress by considering a balance of total tension within the circumferential load carrying thickness and total web thickness:

$$T'^* h_{am} = h_l T', \quad (15)$$

which reflects the fact that the actual in-roll tension stress acts over a proportionally smaller radial differential than the continuum in-roll tension stress.

The strain-displacement and constitutive relationships for the continuum approximation are given by

$$\begin{aligned} \varepsilon'_{\theta\theta} &= \frac{U'}{r} = \frac{T'^*}{E_x^*} + \frac{\nu_{\theta r}^* P'}{E_{ya}} = \varepsilon'_{\theta\theta} + \varepsilon'_{\theta r}, \\ \varepsilon'_{rr} &= \frac{dU'}{dr} = -\frac{P'}{E_{ya}} - \frac{\nu_{r\theta}^* T'^*}{E_x^*} = \varepsilon'_{rr} + \varepsilon'_{r\theta}, \end{aligned} \quad (16)$$

where  $\nu_{\theta r}^*$  and  $\nu_{r\theta}^*$  are the two components of Poisson's ratio relating strain in one direction to strain in the other. In Eq. (16), it has been assumed that the strains from the continuum model represent the actual strains when  $h_l \neq h_{am}$ . This will be true when these strains equal the following alternate expressions:

$$\varepsilon'_{\theta\theta} = \frac{T'}{E_x}, \quad \varepsilon'_{\theta r} = \frac{\nu_{\theta r} P'}{E_{ya}}, \quad \varepsilon'_{rr} = \frac{-P'}{E_{ya}}, \quad \varepsilon'_{r\theta} = \frac{-h_l \nu_{r\theta} T'}{h_{am} E_x}. \quad (17)$$

From Eqs. (15)–(17), the continuum constitutive properties are related to the physical properties of the web ( $E_x$ ,  $\nu_{r\theta}$ , and  $\nu_{\theta r}$ ) by

$$E_x^* = \frac{h_l}{h_{am}} E_x, \quad \nu_{\theta r}^* = \nu_{\theta r}, \quad \nu_{r\theta}^* = \frac{h_l}{h_{am}} \nu_{r\theta}. \quad (18)$$

Strain energy consideration, [3], gives the following relationship between the constitutive properties:

$$\frac{\nu_{\theta r}^*}{E_{ya}} = \frac{\nu_{r\theta}^*}{E_x^*}. \quad (19)$$

Combining Eqs. (14) to (19) yields the following differential equation for the incremental interlayer pressure:

$$r^2 \frac{d^2 P'}{dr^2} + 3r \frac{dP'}{dr} + \left(1 - \frac{h_l E_x}{h_{am} E_{ya}}\right) P' = 0. \quad (20)$$

This is a second-order ordinary differential equation and its solution requires that two boundary conditions be specified. At the periphery of the winding roll, a single winding lap exerts a pressure on the roll that is given by the wound in tension as

$$P'(i) = \frac{t_a(i)}{wr(i)} \quad \text{at the periphery.} \quad (21)$$

At the periphery of the core, since the radial displacement of the core must equal that of the roll, a boundary condition can be written

$$\frac{dP'}{dr} = \frac{2}{c} \left( \frac{E_x h_l}{E_c h_{am}} - 1 + \frac{h_l}{h_{am}} \nu \right) P' \quad \text{at the core/roll interface.} \quad (22)$$

The total pressure in-roll is the sum of total air pressure and total contact pressure if the neighboring layers are in contact:

$$P = P_c + P_g. \quad (23)$$

As the total pressure increases, when more laps are wound, the air pressure, contact pressure, and thus the contact clearance will change as well. Within the roll, the contact pressure and contact clearance  $cc$  are related by Eq. (5). On the other hand, the air pressure in roll is related, by the ideal gas law, to the amount of air entrained while the local lap was being wound:

$$(P_g + p_a)(cc - cc_0 + ca_0) = (P'_g + p_a)ca_w. \quad (24)$$

When winding more laps, the contact clearance between laps in the existing roll can then be updated according to Eqs. (23) and (24).

### 3 Thermal Stress After Winding

Roll winding usually takes place in a temperature-controlled environment where the temperature variation is minimal. After being wound, the rolls are often stored in facilities where the temperature can be significantly different from the winding temperature. In the following we model the effect of temperature changes after winding to in-roll stresses.

After winding, the force equilibrium Eq. (14) still governs the stress distribution in roll. The constitutive relations, including the effect of temperature, are

$$\begin{aligned} \varepsilon'_{\theta\theta} &= \frac{U'}{r} = \frac{1}{E_x^*} T'^* + \frac{\nu_{\theta r}^*}{E_{ya}} P' + \alpha_r F', \\ \varepsilon'_{rr} &= \frac{dU'}{dr} = -\frac{1}{E_{ya}} P' - \frac{\nu_{r\theta}^*}{E_x^*} T'^* + \alpha_r F', \end{aligned} \quad (25)$$

where  $P'$  and  $T'^*$  are the increments of in-roll pressure and tension stress due to the temperature change  $F'(r)$ .

For simplicity, the material properties such as web moduli excluding air and Poisson's ratio are assumed independent of temperature. From Eqs. (18) and (25)

$$\frac{d\varepsilon'_{\theta\theta}}{dr} = \frac{h_{am}}{h_l E_x} \frac{dT'^*}{dr} + \frac{\nu_{r\theta}}{E_x} \frac{dP'}{dr} + \alpha_r \frac{dF'}{dr}. \quad (26)$$

To arrive the above equation, we have assumed the load sharing thickness, web circumferential modulus, coefficient of thermal expansion, and Poissons ratio are invariant with the radius. The variation of  $h_{am}$  with radius is typically very small, and therefore is neglected here. Combining Eqs. (14), (25), and (26) gives the differential equation for the increment in interlayer pressure due to a temperature change

$$r^2 \frac{d^2 P'}{dr^2} + 3r \frac{dP'}{dr} + \left(1 - \frac{h_l E_x}{h_{am} E_{ya}}\right) P' + \frac{h_l}{h_{am}} E_x (\alpha_r - \alpha_t) F' - \frac{h_l}{h_{am}} \alpha_t E_x r \frac{dF'}{dr} = 0. \quad (27)$$

The boundary conditions for the second order ordinary differential Eq. (27) are the following. At the periphery of the wound roll, there is no pressure increment

$$P' = 0 \quad \text{at the periphery.} \quad (28)$$

At the surface of the core ( $r = c/2$ ) the radial displacement continuity due to the local pressure and core temperature change ( $P'_1, F'_1$ ) yields

$$U'_c(c/2) = -\frac{P'_1 c}{2E_c} + \frac{\alpha_c c F'_1}{2}, \quad (29)$$

where  $\alpha_c$  is an equivalent thermal expansion coefficient of the core, and  $E_c$  is the core modulus evaluated at initial temperature and assumed not varying with temperature.

Equation (29) is based on the assumption that the temperature increase within the core is uniform. This is a valid assumption only if heat transfer in the core is much faster than that in the wound roll so that the core reaches thermal equilibrium much faster than the roll.

When Eq. (29) is combined with Eq. (25), it yields the second boundary condition

$$\left. \frac{dP'}{dr} \right|_{r=c/2} = \frac{2}{c} \left[ \frac{E_x h_l}{E_c h_{am}} - 1 + \frac{h_l}{h_{am}} \nu \right] P'_1 + \frac{2h_l}{c h_{am}} E_x (\alpha'_t - \alpha_c) F'_1. \quad (30)$$

Temperature variations after winding change the in-roll pressure, and thus the air pressure, contact pressure, and contact clearance change as well. These in-roll variables can be updated by the same routine as that in the in-roll analysis, except when the temperature effect on air pressure is included, Eq. (24) becomes

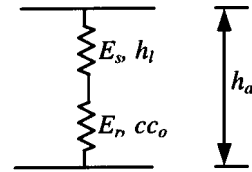
$$\frac{(P'_g + p_a) c a_w}{F_s} = \frac{(P_g + p_a)(cc - cc_0 + ca_0)}{F}, \quad (31)$$

where  $F_s$  is the roll temperature at the start of the thermal analysis. Temperatures  $F$  and  $F_s$  are absolute in reference to  $-273^\circ\text{C}$  ( $-460^\circ\text{F}$ ).

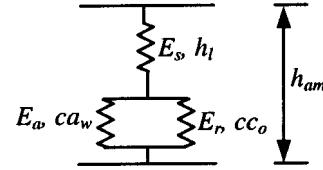
#### 4 Modified Stack Modulus to Include Air and Temperature Effects

In Eq. (19) the stack modulus with the air effect,  $E_{ya}$ , is a modified version of the stack modulus  $E_y$  without air entrainment. The purpose of this section is to develop an expression for  $E_{ya}$  in terms of  $E_y$  and the thickness variables of the model. The analysis first establishes basic definitions where air entrainment is neglected. This is followed by a derivation for the stack modulus where air entrainment between the laps is considered. Finally, a derivation is presented for the stack modulus which additionally includes the temperature effect.

**4.1 Stack Modulus Excluding Air Entrainment.** Consider part (a) of Fig. 2, which shows incipient contact of two webs in a vacuum. In this figure, the reference web thickness is the total web thickness  $h_a$ , and the contact reference clearance is  $cc_0$ . The total web thickness,  $h_a$ , can be broken into two layers, one of which is the support with reference thickness  $h_l$  and bulk modulus  $E_s$ , and the other is the layer consisting of surface roughness with reference thickness  $cc_0$  and modulus  $E_r$ . When air is excluded, these two layers are modeled as elastic springs linearly connected in series (Fig. 4(a)). The stack modulus of the total web excluding air is



(a) Excluding air effect.



(b) Including air effect.

Fig. 4 Stack modulus

$$E_y = \frac{h_a E_r E_s}{cc_0 E_s + h_l E_r}. \quad (32)$$

The above equation can be solved for the roughness modulus  $E_r$  if the stack modulus  $E_y$ , bulk modulus  $E_s$ , and reference thickness of each layer are available.

**4.2 Stack Modulus Including Air Entrainment.** Next, consider parts (b) and (c) of Fig. 2 that shows the relative position of the outermost two laps after the outer lap has passed onto the wound roll. In this figure, the reference web thickness,  $h_{am}$ , is now the total web thickness including the effect of air entrainment and the effect of roughness if contact occurs under the outer lap such as shown in Part (b) of Fig. 2. The contact reference clearance is now  $cc_w$ , and air film reference is  $ca_w$ . These quantities are computed in the outer lap analysis.

The air trapped in the roughness area between two laps will affect the compressibility of the roll. When air is included, the roughness area is modeled as two springs in parallel (Fig. 4(b)); one represents the roughness surface with reference thickness  $cc_0$  and modulus  $E_r$ , and the other represents the air film reference thickness  $ca_w$  and modulus  $E_a$ . The total web is modeled as this roughness layer and the support layer (reference thickness  $h_l$  and bulk modulus  $E_s$ ) connected in series. The air film modulus is from the compressibility of the air. When air leakage through the sidewall is excluded and the air follows the ideal gas law, the air film modulus is, [6],

$$E_a = \frac{(P_g + p_a)^2}{(P'_g + p_a)}. \quad (33)$$

The stack modulus of the total web is then

$$E_{ya} = \begin{cases} \frac{h_{am}}{\frac{h_l}{E_s} + \frac{ca_w}{E_a}} & \text{when the laps are not in contact} \\ \frac{h_{am}}{\frac{h_l}{E_s} + \frac{1}{\frac{E_a}{ca_w} + \frac{E_r}{cc_0}}} & \text{when the laps are in contact} \end{cases}. \quad (34)$$

In the in-roll stress analysis, before the  $i$ th lap is added, the stack modulus is computed along the radius in the winding roll. This is done at each radial location as follows. First, the roughness interface modulus is computed using Eq. (32). Then Eq. (34) is

**Table 1 Winding conditions and results from experiments and model predictions**

Test #	Speed, m/s	Start tension per width, N/m	Finish tension per width, N/m	Nip force per width, N/m	Accel at cinching, m/s <sup>2</sup>	Torque per width at core, N	Contact pressure at core, kPa	Contact pressure at core from model, kPa
1	4.3	622	263	263	0.76	572	73	97
2	4.3	727	306	263	>1.02	>762	>97	104
3	4.3	832	350	263	>1.02	>762	>97	108
4	5.1	727	306	263	1.02	762	97	102
5	5.1	766	766	263	1.02	762	97	103
6	5.1	832	350	263	>1.02	>762	>97	106

used to evaluate the stack modulus with the air entrainment effect included. Once the stack modulus is known, the incremental in-roll solution for the  $i$ th lap can be found. Finally, the cumulative in-roll solution is determined.

**4.3 Stack Modulus Including Air Entrainment and Thermal Effect.** We assumed the support and roughness moduli do not vary with temperature in the temperature range of interest. With this assumption, the effect of temperature on stack modulus depends solely on  $E_a$ , the modulus of the air film. Using the ideal gas law under isothermal expansion, the air film modulus is

$$E_a = \frac{(P_g + p_a)^2 F_s}{(P'_g + p_a) F} \quad (35)$$

Then the stack modulus, including air entrainment and temperature effect, is available by substituting the above equation into Eq. (34).

**4.4 Stack Modulus Measurement and Data Reduction.** In order to perform numerical simulations using the winding model, several material properties and geometric parameters must be measured empirically. Some of these are measured conventionally (e.g., Young's modulus of the web); however, several new variables have been introduced and so some discussion on how to measure them is now provided.

The new material properties required of the model include the underlying support modulus and the roughness modulus as defined in Eq. (32). To obtain these parameters, the circumferential load carrying thickness and the total web thickness must be known as well. The total web thickness is the sum of the load sharing thickness and the contact reference clearance. It is determined from experimental stack modulus measurements as follows. First, three stacks of support are constructed from individual plies having an area of 1.27 cm by 5.08 cm. The number of plies within each stack is chosen such that the height is 0.51 cm. Each of the three stacks is sequentially placed between two parallel plates and compressed to a small preload of 103 Kpa. The load is then reduced to 13.8 KPa and the height of each stack noted via the average output from three LVDT's located at 120° increments around the perimeter of the upper and lower platens. The total stack height is divided by the number of individual plies and the resulting thickness is averaged from the three separate measurements to yield the total web thickness.

Following this measurement, each stack is then compressed at a constant strain rate of 0.51 mm/min up to a final stress of 12.4 MPa. Displacements are measured as the average output of the three LVDTs and stress is measured using a load cell. From this data, the radial compressive modulus excluding air is computed since the stack area is sufficiently small enough to mitigate the air effect during compression. The bulk modulus is determined by computing the tangent modulus from the stress-strain data near the upper end of the stress range. Presumably, at the higher stresses, the roughness interface has been significantly compressed and the stress-strain behavior is predominately governed by the bulk modulus.

Finally, the roughness modulus is computed by inverting Eq. (32) once the contact reference clearance is known. As previously mentioned, the contact reference clearance is determined from the root-mean-square of the front and backside  $R_z$  (measured via the Wyko®).

## 5 Numerical Solution

The solution of the above model was obtained numerically. The numerical algorithm "winds" one lap after another onto the "core" until the last lap is wound. During winding of each individual lap, the algorithm is as follows:

1. *Pressure roller nip analysis:* Given the nip load, winding speed, web reference clearances, and roll/pressure roller geometry, the equivalent radius and equivalent modulus of the roll/pressure roller are evaluated. Then Eqs. (1) to (5) are solved by Newton's iterative method for the contact force  $f_c(i)$ , air force  $f_a(i)$ , contact clearance  $cc_n(i)$ , and air film clearance  $ca_n(i)$  under the nip.
2. *Internal outer lap analysis:* The contact force from the step 1 is used to obtain the nip induced tension and wound-in-tension. Then Eq. (9) is used to evaluate  $ca_a(i)$ , the air film clearance under the outer lap away from the nip adjusted to the atmospheric pressure. Equations (8), (10), and (11) are solved afterwards to obtain the contact clearance  $cc_w(i)$ , the contact pressure  $P'_c(i)$ , and air pressure  $P'_g(i)$  under the outer lap away from the nip.
3. *In-roll analysis:* The stack moduli including the air effect are first evaluated using the in-roll conditions. Central finite difference method is then applied to solve the ordinary differential Eq. (20) with the boundary conditions (21) and (22).
4. *Roll profile and stress update:* Results from step 3 are used to update the roll profile and in-roll stress distribution.
5. *Repeat:* Steps 1 to 4 are repeated until all laps are wound onto the roll.
6. *Thermal stress analysis after winding:* The nonlinear boundary value problem of the thermal stress analysis (Eq. (27)) is solved by Newton's iterative method.

## 6 Experimental Verification and Parametric Study

**6.1 Experiments.** Experiments are conducted in the Kodak conveyance and winding laboratory. The experiments consisted of winding a sequence of polymer-coated paper (224  $\mu$ m thick and 7925 m long, roll OD 1.5 m) onto 0.127 m (5 inch) outer diameter cardboard cores. Test rolls are wound with a pressure roller force of 263 N/m (1.5 pli) contact force under two levels of speed, 4.3 and 5.1 m/s (850 and 1000 fpm), and five levels of tension profile, as detailed in Table 1. The tension profiles, with the exception of test 5, which is at constant tension, are linearly tapered with the length of the web wound onto the roll.

After winding, the rolls are tested to evaluate the torque transmission capability. Before testing, straight lines are drawn on both sides of every test roll. Then the rolls are repeatedly accelerated up to 5.1 m/s (1000 fpm) using incremental acceleration rates and then stopped. The acceleration rate starts at 0.25 m/s<sup>2</sup> (50 fpm/

**Table 2 Material properties used in modeling**

$c$ (m)	0.127	$E_x$ (MPa)	5720	$\nu$	0.02	$E_s$ (MPa)	179
$ca_o$ ( $\mu\text{m}$ )	8.387	$h_d$ ( $\mu\text{m}$ )	235	$E_p$ (MPa)	2	density, $\text{kg/m}^3$	1107
$cc_o$ ( $\mu\text{m}$ )	10.64	$h_l$ ( $\mu\text{m}$ )	224	$r_p$ (m)	0.0762	roll OD, m	1.5
$E_c$ (MPa)	410	$\mu_w$	0.31	$v_p$	0.495	lap number	3089

sec), and then increases up to 1.02 m/s<sup>2</sup> (200 fpm/sec) in 0.25 m/s<sup>2</sup> increments. The rolls are then decelerated at a much gentle deceleration rate of 0.05 m/s<sup>2</sup> (10 fpm/sec). After rolls are stopped, they are checked for cinches (circumferential breaks of the straight lines on both ends). Results are shown in Table 1, from which half of the six rolls do not cinch at 1.02 m/s<sup>2</sup>, the maximum acceleration capability of the lab equipment. Among the three rolls that cinched, one cinched at 0.76 m/s<sup>2</sup> (150 fpm/sec), and two cinched at 1.02 m/s<sup>2</sup>. For all of these three rolls, cinching takes place near the core. The acceleration rate when cinching starts can be used to estimate the contact pressure at the core. In this calculation, it is assumed that it is the contact pressure that provides the roll with torque transmission capability. The contact pressures at the core from the cinch tests are shown in Table 1.

**6.2 Model Predictions.** The computer program described above is used to predict the in-roll stress distribution of rolls wound at the winding conditions listed in Table 1. Key inputs to the model are summarized in Table 2, and the relationship among contact clearance, contact pressure, and roughness modulus from testing of the same polymer coated paper is listed in Table 3. From the model prediction, the contact pressures at the core at different winding conditions are listed in Table 1, and they agree fairly well with the respective contact pressures from the torque transmission tests.

When using the winding conditions of test 1 in Table 1, the total interlayer pressure, contact pressure, and air gage pressure distribution after winding are shown in Fig. 5. For comparison purposes, the interlayer pressure from a nonair entrainment model is also included. With the air entrainment effect, the total pressure is the sum of contact pressure and air pressure, the former of which is supported by roughness contact of two neighboring laps and the later from air gage pressure. The result indicates the existence of a core zone where the total pressure and gage pressure start at low values and then rapidly increase to peak pressures. Further out in the roll, the total pressure and gage pressure fall and become close to zero at the finished roll surface. The presence of the core zone is mostly due to the soft cardboard core, which results in a low core modulus, thus resulting in a sharp drop in the pressures at the core. In winding and in downstream unwinding, the torque from the core is transmitted from the inner laps to the outer laps by a friction force induced by direct contact pressure. The contact pressure at the core therefore determines the local torque transmission capability. The interlayer pressure from the non-air entrainment model is higher than the contact pressure but lower than the total interlayer pressure from the air entrainment model.

Figure 6 shows the interlayer tension, wound-in-tension, and machine tension stress distributions. Again, the interlayer tension

**Table 3 Roughness modulus of the polymer coated paper excluding air effect**

Contact Clearance, $\mu\text{m}$	Contact Pressure, MPa	Stack Modulus, MPa
10.640	0.000	0.021
4.933	0.014	0.083
3.896	0.028	0.227
3.416	0.041	0.396
2.210	0.138	1.609
1.380	0.345	4.326
0.798	0.689	8.887
0.282	1.379	20.057
0.016	2.413	69.154

from the non-air entrainment model is included for comparison purposes. Because of the low core modulus when the air effect is included, the interlayer tension stress near the core is highly negative, which could potentially cause local buckling. The wound-in-tension (tension in the outer lap downstream of the pressure roller) is higher than the machine tension (tension upstream of the pressure roller) due to the friction force induced by the pressure load underneath the pressure roller nip. The interlayer tension stress from the nonair entrainment model is different than that from the air entrainment model, and in this example does not show a region of sharp change near the core.

The contact clearances under the pressure roller, under the outer lap away from the nip, and after winding are shown in Fig. 7. All clearances are lower than the reference contact clearance  $cc_o$  and air film reference clearance  $ca_o$ . This indicates that throughout

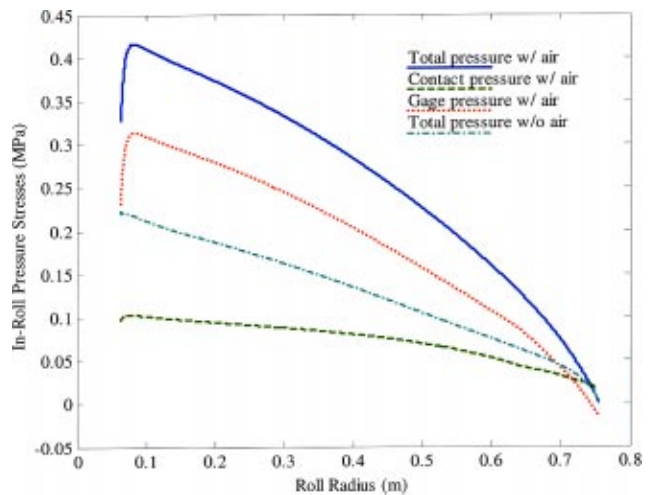


**Fig. 5 In-roll pressure stresses right after winding from both air entrainment model and nonair entrainment model. The gage pressure is the air pressure above the ambient pressure.**

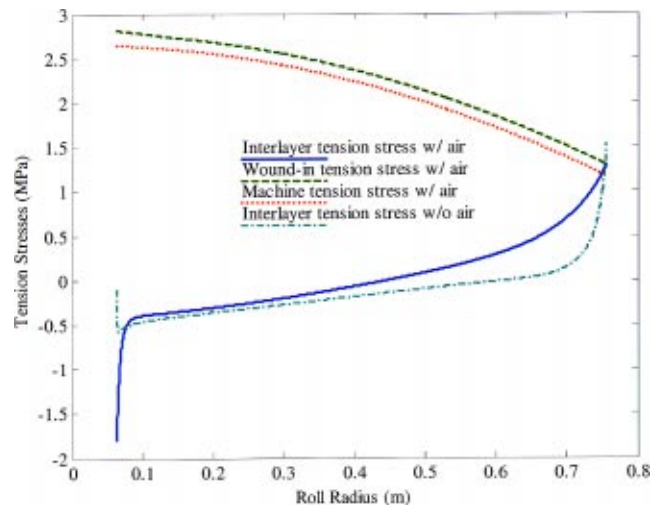


**Fig. 6 In-roll tension stresses right after winding from both air entrainment model and nonair entrainment model**

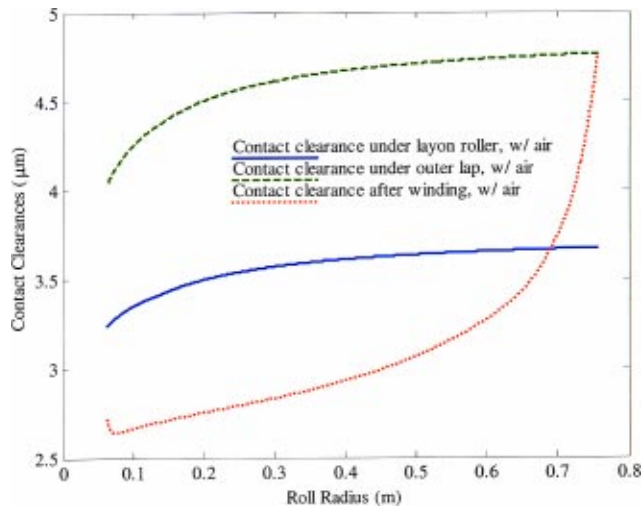


Fig. 7 Contact clearances under the pressure roller, under the outer lap away from the nip, and after winding

the winding process, no laps are floating or are purely supported by air pressure. The contact clearance under the outer lap is below the contact reference clearance due to the existence of the pressure roller, which squeezes out most of the air under the nip and only lets a small amount of entrapped air into the roll. Contact clearance under the outer lap away from the nip is higher than that under the pressure roller, which suggests that right after being compressed by the pressure roller nip, the air under the outer lap expands. Depending on how much air passes through the nip and the wound-in-tension, the gage pressure could be negative under the outer lap away from the pressure roller nip, resulting in sub-ambient air pressure locally.

**6.3 Thermoelastic Effect.** After winding, the rolls are usually put into storage before unwinding. The typical storage time varies from hours to years. Often, rolls are stored in nontemperature controlled warehouses where the roll temperature varies with the season. In some manufacturing processes, rolls are intentionally stored at elevated temperatures for a specific time to control certain web properties (such as core set curl). In-roll stress changes with roll temperature mostly because the coefficient of thermal expansion (CTE) of the web is anisotropic, and the core CTE is different than that of the web. The interlayer pressure increases at elevated temperature when the CTE along the radial direction is higher than that of the circumferential direction because the roll expands more along the radial direction than the hoop direction.

In the following, the temperature effect on wound roll stress is studied by assuming the roll is wound using test 1 (Table 1) winding conditions at an ambient temperature of 70°F, and after winding there is a step change in roll temperature from 70°F to 100°F. After the temperature change, the total interlayer pressure and contact pressure from the air entrainment model are shown in Figs. 8 and 9 at three levels of radial coefficient of thermal expansion,  $\alpha_r = 10^{-5}$ ,  $10^{-4}$ , and  $10^{-3}$  (1/°F). Other coefficients of thermal expansion are fixed at  $\alpha_\theta = 10^{-5}$  1/°F tangentially for the web, and  $\alpha_c = 10^{-4}$  1/°F for the core. As shown in Figs. 8 and 9, the total interlayer pressure is much more sensitive to the radial CTE than the contact pressure. This indicates that the increase in total interlayer pressure is mostly from the increase in gage pressure (the difference between the total interlayer pressure and contact pressure), which is due to both a higher temperature and a lower air gap.

When using the non-air entrainment model, the temperature effect to interlayer pressure is given in Fig. 10, which shows the

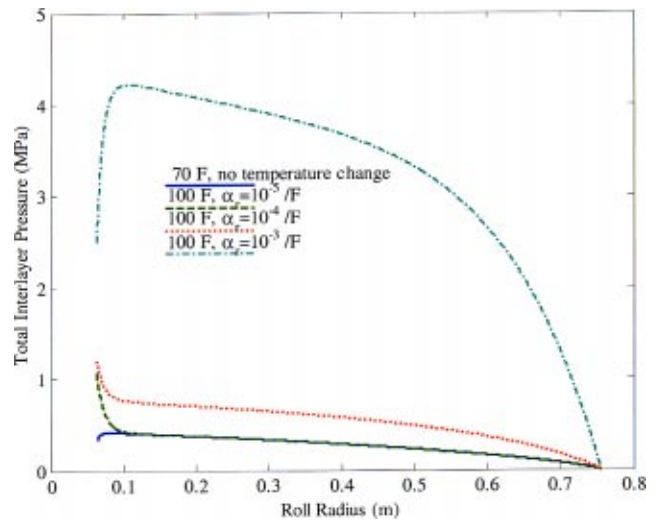


Fig. 8 The effect of roll radial CTE on total interlayer pressure right after winding at 70°F and after heated to 100°F. Results are from the air entrainment model. The radial CTE of the roll is indicated in the figure. Other CTEs are  $\alpha_\theta = 10^{-5}/^\circ\text{F}$  and  $\alpha_c = 10^{-4}/^\circ\text{F}$ .

effect of temperature change on interlayer pressure is similar to the total interlayer pressure when the air effect is included.

Besides the thermal expansion coefficient of the web, the wound roll stress is also affected by the thermal expansion coefficient of the core. At a temperature change from 70°F to 100°F, Figs. 11 and 12 give the model predictions of the total interlayer pressure and contact pressure at three levels of core coefficient of thermal expansion,  $\alpha_c = 10^{-5}$ ,  $10^{-4}$ , and  $10^{-3}$  (1/°F). Web coefficients of thermal expansion are fixed at  $\alpha_r = 10^{-4}$  1/°F radially and  $\alpha_\theta = 10^{-5}$  1/°F tangentially. When using the nonair entrainment model, the results are shown in Fig. 13. From the predictions, the core effect is only localized to the laps close to the core. A higher core thermal expansion coefficient than the web would enhance the thermal stress effect, and make the local in-roll pressure even higher when heated, and even lower when cooled.

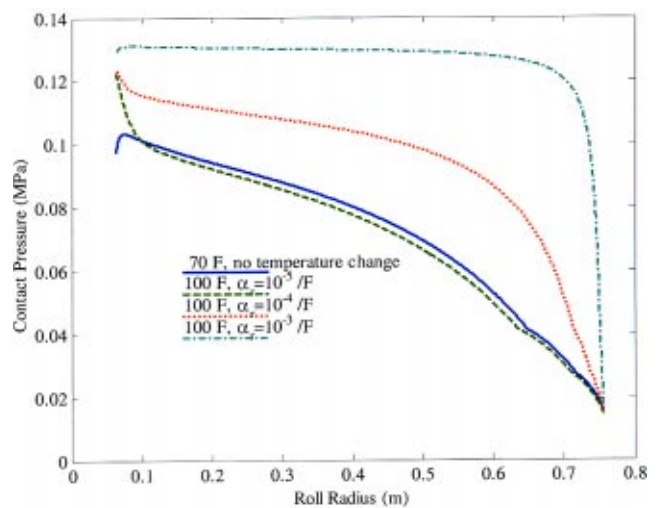


Fig. 9 The effect of roll radial CTE on contact pressure right after winding at 70°F and after heated to 100°F. Results are from the air entrainment model. The radial CTE of the roll is indicated in the figure. Other CTEs are  $\alpha_\theta = 10^{-5}/^\circ\text{F}$  and  $\alpha_c = 10^{-4}/^\circ\text{F}$ .

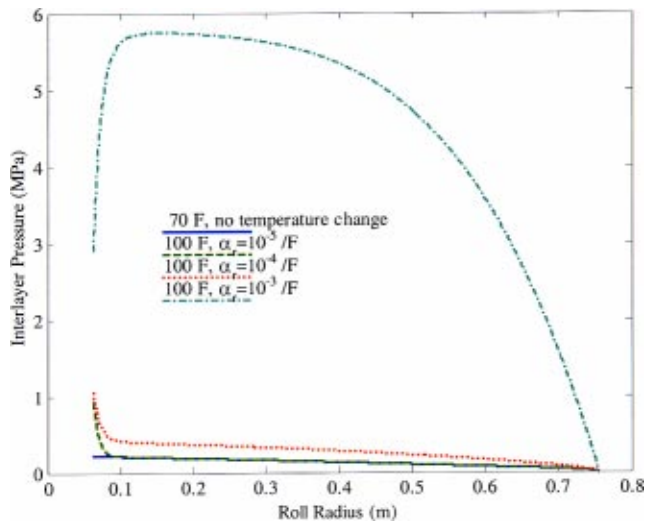


Fig. 10 The effect of roll radial CTE on interlayer pressure right after winding at 70°F and after heated to 100°F. Results are from the nonair entrainment model. The radial CTE of the roll is indicated in the figure. Other CTEs are  $\alpha_\theta = 10^{-5}/^\circ\text{F}$  and  $\alpha_c = 10^{-4}/^\circ\text{F}$ .

## 7 Model Limitations

The model presented in this paper neglects the effect of side leakage both during and after winding. As the experimental results indicate, reasonable agreement is obtained for a specific test case. However, as process conditions are changed, it is expected that this assumption will no longer be valid. For example, as web width is decreased, the air under the outer lap will be more significantly affected by the atmospheric boundary conditions at either end of the roll. To further investigate the quantitative impact of this limitation, a simple theory was developed to establish time scales for air leakage from a wound roll and is presented in the Appendix.

Results from the analysis are presented in Figs. 14 and 15. These figures give a plot of the percentage of original air mass lost from the first lap of the roll (nearest the core) as a function of the

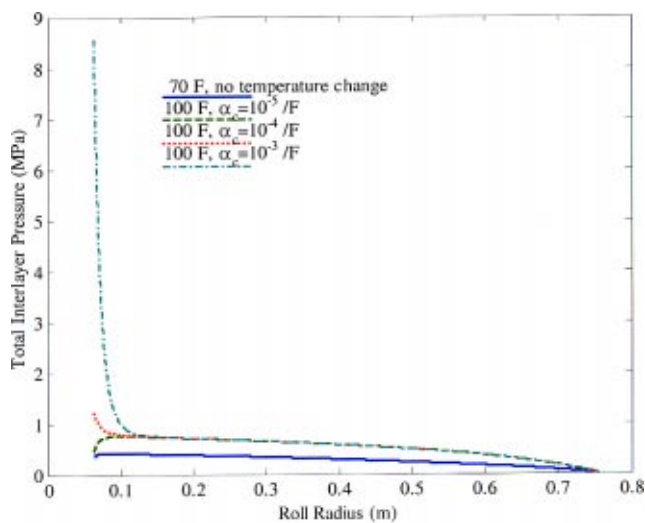


Fig. 11 The effect of roll core CTE on total interlayer pressure right after winding at 70°F and after heated to 100°F. Results are from the air entrainment model. The core CTE of the roll is indicated in the figure. Other CTEs are  $\alpha_r = 10^{-4}/^\circ\text{F}$  and  $\alpha_\theta = 10^{-5}/^\circ\text{F}$ .

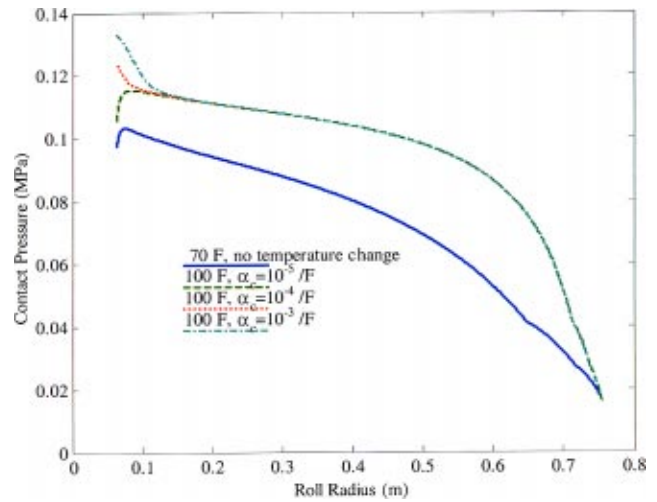


Fig. 12 The effect of roll core CTE on contact pressure right after winding at 70°F and after heated to 100°F. Results are from the air entrainment model. The core CTE of the roll is indicated in the figure. Other CTEs are  $\alpha_r = 10^{-4}/^\circ\text{F}$  and  $\alpha_\theta = 10^{-5}/^\circ\text{F}$ .

initial clearance and the web width. The results are computed at the completion of winding and indicate that wider webs with smaller initial clearances have smaller air leakage and that less air leakage occurs at higher winding speeds. For example, as indicated in the Appendix, the initial clearance under the lap nearest the core after the 4th lap of the roll is added is equal 1.464  $\mu\text{m}$ . This corresponds to results from test 1 from Table 1. Using these values and the web width in test 1, the percentage of air mass lost under the lap nearest the core at the completion of winding is between 25 and 40%. While this magnitude of air loss is significant, it is cumulative over the winding duration and therefore probably does not invalidate the winding model since the impact of added laps to interlayer pressure is localized to laps in the vicinity of the radial location of interest.

However, since even more air will leak out of the roll after winding, the subsequent assumption of no side leakage during the thermoelastic portion of the analysis is probably invalid. This sug-

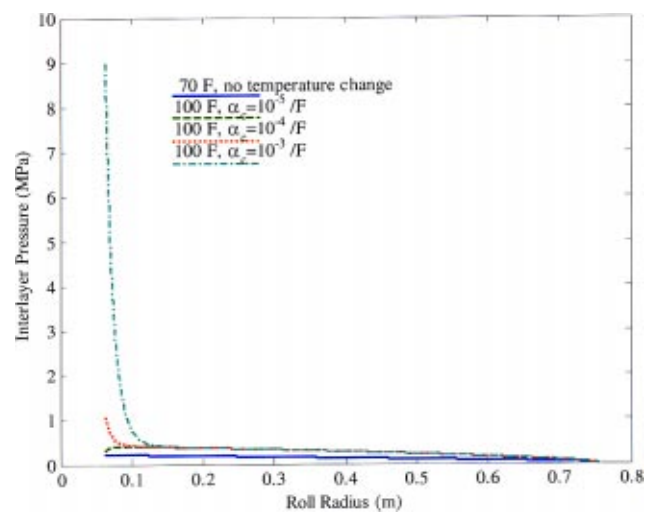


Fig. 13 The effect of roll core CTE on interlayer pressure right after winding at 70°F and after heated to 100°F. Results are from the nonair entrainment model. The core CTE of the roll is indicated in the figure. Other CTEs are  $\alpha_r = 10^{-4}/^\circ\text{F}$  and  $\alpha_\theta = 10^{-5}/^\circ\text{F}$ .

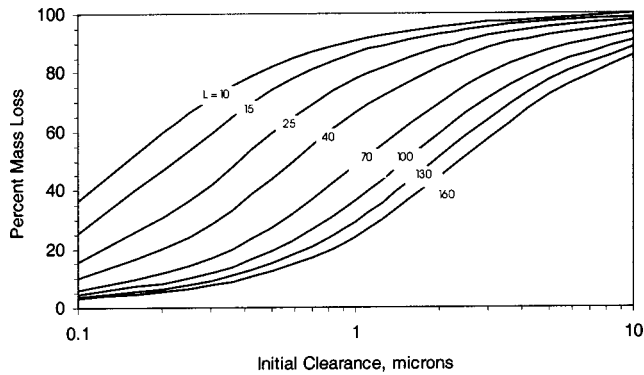


Fig. 14 Total mass of air lost from the first lap of a roll after winding 3089 laps at 2.54 m/s (500 ft/min), expressed as a percentage of the original mass in the lap. The half-width of the roller in centimeters,  $L$ , is indicated on the figure. Data are presented here for a core having outer diameter of 0.127 m (5 inches), and for a web thickness of 224  $\mu\text{m}$ .

gests that for the range of speeds and for the web width considered in this study that the no side leakage assumption is not reasonable. However, as the web width is increased, the assumption is better met and in the limit for a very wide web, our thermoelastic results will be accurate. Therefore, for many practical web winding simulations, side leakage needs to be incorporated into the winding model. However, this will introduce much more complexity into the model and will be expected to be numerically intensive.

## 8 Conclusions

An air entrainment model was developed. The model includes a web roughness model, a pressure roller nip analysis, an outer lap analysis, and an in-roll analysis. In addition, the effect of temperature on thermoelastic stresses after winding is included. The winding model gives reasonable predictions compared with winding experiments on polymer coated paper. The parametric study showing the effect of CTEs on in-roll stress is also presented. Comparison to previous models excluding air entrainment indicates a very significant reduction in contact interlayer pressure caused by the trapped air. The model does not include side leakage during and after winding. An analysis was developed indicating the range over which this assumption is valid. Future modeling will be extended to include the effect of side leakage.

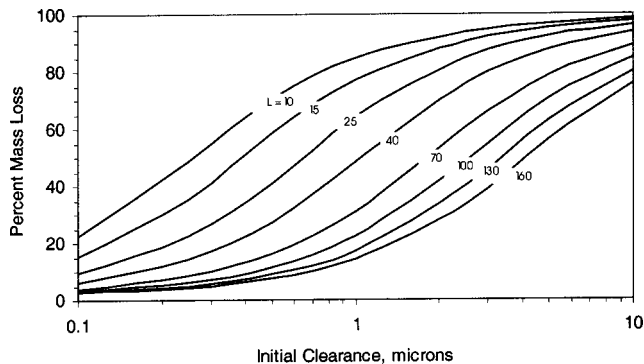


Fig. 15 Total mass of air lost from the first lap of a roll after winding 3089 laps at 7.62 m/s (1500 ft/min), expressed as a percentage of the original mass in the lap. The half-width of the roller in centimeters,  $L$ , is indicated on the figure. Data are presented here for a core having outer diameter of 0.127 m (5 inches), and for a web thickness of 224  $\mu\text{m}$ .

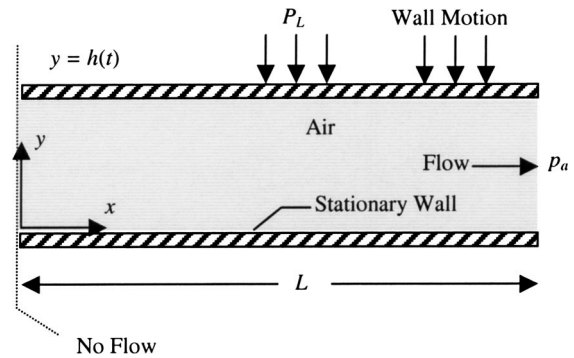


Fig. 16 Geometry for lubrication analysis of squeezing flow

## Appendix

**Air Leakage in Winding.** The purpose of this appendix is to set forth a simple theory that establishes time scales for air leakage from a wound roll under a tensile load. The results of this theory may be used to demonstrate the validity of various assumptions used in winding models, which often involve issues regarding air leakage out of the widthwise edges of a roll while winding is occurring. The incorporation of air leakage into a winding model introduces much complexity and is numerically intensive; as such, the subsequent analysis can justify when the added complexity is necessary, and when a simpler nonleakage model is adequate.

**Theory of Air Loss.** We first consider a simple one-dimensional lubrication model for the “squeezing” of air out of a gap as it closes under a constant external load. This is to model the approximate air loss occurring on any single lap of the roll. We then provide some limiting cases of the lubrication model. Lastly, we show how the model is used to approximate the cumulative air loss in a given lap as more laps are added to a roll.

Consider the configuration shown in Fig. 16 in which walls bound a region containing air. The  $x$ - $y$  coordinate system is as indicated, and the  $z$ -direction extends out of the figure. The domain has length  $L$ ; we assume that the flow is invariant in the  $z$ -direction. At the location  $x=0$ , we assume that there can be no flow, and at  $x=L$ , we assume that the air pressure is atmospheric,  $p_a$ . We assume that the top wall of the domain is entirely flat and is set in motion due to a pressure difference between an external pressure load  $P_L$ , and an initial air pressure in the gap,  $P_H$ . We parameterize the moving top wall location as  $y=h(t)$ , while the bottom wall at  $y=0$  remains stationary. As a result, the internal air generates a pressure field  $P(x,t)$  that opposes this load, and there is a resulting air flow exiting from the domain at  $x=L$ . We assume that the air obeys a polytropic relation between the local density  $\rho$  and pressure, i.e.,

$$\rho = c P^{1/\gamma}, \quad (A1)$$

where  $c$  and  $\gamma$  are constants. For isothermal compression,  $\gamma=1$ , while for adiabatic compression,  $\gamma=C_p/C_v$ , where  $C_p$  and  $C_v$  are the respective heat capacities at constant pressure and volume ( $\gamma \sim 1.4$  for air); the flow is incompressible in the limit as  $\gamma$  approaches infinity. We further assume that inertial effects are negligible, and that the assumptions of lubrication theory are valid. These two assumptions are satisfied, provided

$$\frac{h_0}{L} \ll 1, \quad \left( \frac{\rho_0 Q_s}{\mu} \right) \left( \frac{h_0}{L} \right) \ll 1, \quad (A2)$$

where  $h_0$  and  $\rho_0$  are characteristic scales for the gap clearance and density, respectively; we choose these quantities as  $h(t=0)=h_0$  and  $\rho(t=0)=\rho_0$ .  $Q_s$  is a volumetric flow per width scale given in (A3g). Our goal is to determine the pressure field in the small

gap, the location of the top surface  $h(t)$ , and the mass of air exiting the domain to atmosphere as a function of time.

With the above stated assumptions, the dimensionless system governing the location of the moving wall and internal pressure is given by

$$\frac{\partial}{\partial t}(\bar{h}\bar{P}^{1/\gamma}) + \frac{\partial}{\partial \bar{x}}(\bar{P}^{1/\gamma}\bar{Q}) = 0, \quad (A3a)$$

$$\bar{Q} = -\bar{h}^3 \frac{\partial \bar{P}}{\partial \bar{x}}, \quad (A3b)$$

$$\int_0^1 \bar{P} d\bar{x} = 1, \quad (A3c)$$

$$\bar{P} = \bar{P}_H, \quad \bar{h} = 1, \quad \text{at } \bar{t} = 0, \quad (A3d)$$

$$\frac{\partial \bar{P}}{\partial \bar{x}} = 0 \quad \text{at } \bar{x} = 0, \quad (A3e)$$

$$\bar{P} = \bar{P}_A \quad \text{at } \bar{x} = 1, \quad (A3f)$$

where

$$\begin{aligned} \bar{P} &= \frac{P}{P_L}, \quad \bar{P}_H = \frac{P_H}{P_L}, \quad \bar{P}_A = \frac{P_A}{P_L}, \quad \bar{x} = \frac{x}{L}, \quad \bar{t} = \frac{t}{t_s}, \\ \bar{Q} &= \frac{Q}{Q_s}, \quad t_s = \frac{12\mu L^2}{h_0^3 P_L}, \quad Q_s = \frac{h_0^3 P_L}{12\mu L}. \end{aligned} \quad (A3g)$$

As indicated in (A3), our convention is that overbars denote dimensionless variables. In (A3),  $\bar{Q}$  is the dimensionless volumetric flow rate per unit width. The above system (A3) is standard, except for the integral constraint (A3c) that balances forces on the moving wall. Note that in keeping with the constraints of lubrication theory, we have also neglected inertial effects in (A3c). The system (A3) is well posed to solve for the pressure and web location.

Of particular interest is the mass exiting the domain to atmosphere at  $\bar{x} = 1$ . We determine this quantity as follows. First, the Eq. (A3a) is integrated in  $\bar{x}$  between the limits 0 and 1 using the pressure boundary conditions in (A3e) and (A3f) to obtain

$$\bar{Q}|_{\bar{x}=1} = -\frac{1}{\bar{P}_A^{1/\gamma}} \frac{\partial}{\partial \bar{t}} \left( \bar{h} \int_0^1 \bar{P}^{1/\gamma} d\bar{x} \right). \quad (A4a)$$

The expression (A4a) yields the volumetric flow rate existing the domain. Since the flow is compressible, the mass flow rate,  $\bar{Q}_m$ , is the useful quantity. Using the density given by (A1), the relation between the dimensionless mass and volumetric flow rate can be expressed as

$$\bar{Q}_m = \bar{P}_A^{1/\gamma} \bar{Q}, \quad \bar{Q}_m = \frac{Q_m}{c P_L^{1/\gamma} Q_s}, \quad (A4b)$$

and thus

$$\bar{Q}_m|_{\bar{x}=1} = -\frac{\partial}{\partial \bar{t}} \left( \bar{h} \int_0^1 \bar{P}^{1/\gamma} d\bar{x} \right). \quad (A4c)$$

The result (A4c) is integrated over time to yield the total mass per unit width that has left the domain at any time  $t$ ,  $M(t)$ . Using the initial condition (A3d), we thus obtain

$$\begin{aligned} \bar{M}(\bar{t}) &= \bar{P}_H^{1/\gamma} - \bar{h}(\bar{t}) \int_0^1 \bar{P}(\bar{x}, \bar{t})^{1/\gamma} d\bar{x}, \quad \bar{M}(\bar{t}) = \frac{M}{M_s}, \\ M_s &= c P_L^{1/\gamma} h_0 L. \end{aligned} \quad (A4d)$$

The original mass in the domain per unit width,  $M_0$ , can be expressed in dimensionless form using the density (A1), initial condition (A3d), and the dimensionless scaling for mass  $M_s$  given in (A4d) as

$$\bar{M}_0 = \bar{P}_H^{1/\gamma}. \quad (A4e)$$

Finally, combining (A4d) and (A4e), we obtain the desired expression for the fraction of the original mass lost at any time as

$$\frac{M(t)}{M_0} = \frac{\bar{M}(\bar{t})}{\bar{M}_0} = 1 - \frac{\bar{h}(\bar{t})}{\bar{P}_H^{1/\gamma}} \int_0^1 \bar{P}(\bar{x}, \bar{t})^{1/\gamma} d\bar{x}. \quad (A4f)$$

This concludes our derivation of the squeezing flow problem.

A numerical solution of (A3) is required except in certain limiting cases. To proceed, a new variable  $U = \bar{h}\bar{P}^{1/\gamma}$  is introduced into (A3). The resulting system is then solved using finite differences with a Crank-Nicholson implicit scheme, and a full Newton iteration at each time step.

An analytic solution to (A3) can be obtained for the limiting case of an incompressible fluid, for which  $\gamma \rightarrow \infty$  in (A1). Under such circumstances the  $\bar{P}^{1/\gamma}$  terms in (A3a) are lost. Then, since  $\bar{P} = \bar{P}(\bar{x}, \bar{t})$  and  $\bar{h} = \bar{h}(\bar{t})$ , Eqs. (A3a) with (A3b) are separable and can be integrated; after subsequent application of the boundary conditions in (A3) we obtain

$$\bar{h} = [1 + 6(1 - \bar{P}_A)\bar{t}]^{-1/2}, \quad (A5a)$$

$$\bar{P} = \frac{3}{2}(1 - \bar{P}_A)(1 - \bar{x}^2) + \bar{P}_A. \quad (A5b)$$

We note here that (A5b) does not satisfy the initial pressure condition in (A3d); an incompressible fluid instantaneously yields the pressure field (A5b) underneath the closing gap for all times. There is no finite transient in pressure as can be obtained in the case of a compressible fluid. For an incompressible fluid, the expression (A4f) for the fraction of the original mass lost from the domain becomes

$$\frac{M(t)}{M_0} = 1 - \bar{h}(\bar{t}), \quad (A5c)$$

which is identical to the fraction of the volume lost as expected.

On the other hand, for cases of negligible flow,  $\bar{Q} \rightarrow 0$  in (A3a), and the system (A3) yields the simple result that

$$\bar{h}\bar{P}^{1/\gamma} = K, \quad (A6)$$

where  $K$  is a constant. This case corresponds to the situation where there is no air leakage from the domain, and the pressure field is constant everywhere.

We now consider how the preceding model may be used to approximate the air leakage in a winding roll. To proceed, we assume that the air flow variations in the direction of the web motion are small compared with those across the width of the web. Thus, we focus attention solely on the air flow occurring in the widthwise direction towards the edges of the web. The no flux condition located at  $x=0$  in Fig. 16 is interpreted as a symmetry condition for the roll width; thus, the computational length of the domain,  $L$ , is taken to be half of the roll width. We fix our view on a given lap in the roll, and track the mass of air lost in that particular lap as additional laps are added. Since the first lap (i.e., at the core) has the longest time available for air leakage and generally experiences the highest pressure loading, the cumulative amount of air leakage is the largest of all laps. For this reason, we examine the first lap in this appendix. We assume that when the first lap is an outer lap of the roll, it experiences a constant load (due to the roll tension) until one revolution of the roll occurs, at which time a second lap begins to be wound. At this point, there is an instantaneous pressure load increase on the original lap, which

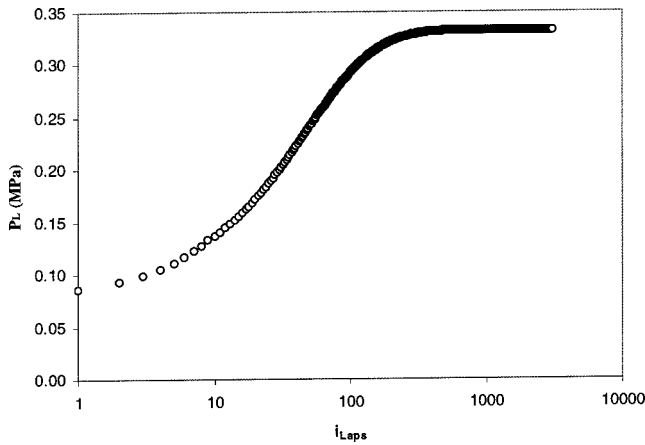


**Fig. 17** Calculated absolute air pressures under the first lap (circles) from full winding model. These air pressures are used to model the air loss under the first lap.

again remains constant for the whole lap. This procedure is continued as more laps are added. For a web moving at speed  $V$ , the time to complete a revolution,  $t_R$ , is given by

$$t_R = \frac{2\pi(r + (i-1)h_a)}{V} \quad (A7)$$

Thus, in (A7), any given pressure load is applied for the length of time  $t_R$ .

A relation between the load pressure,  $P_L$ , and the number of laps being wound onto the roll,  $i$ , is required so that (A3) may be solved on each lap. One such relationship may be obtained via a simple membrane theory between pressure and tension in which there is no contact between laps as additional laps are added. A more realistic pressure load model incorporates the effect of web-to-web contact, which tends to reduce the pressure load on the air. To obtain such an expression, the full winding model detailed in this report was utilized; as in the case of our air leakage model, the full winding model assumes that the pressure load remains constant until a new lap is added. Although this relationship generally changes as winding conditions are altered, we simplified our calculations by obtaining a single relationship between  $P_L$  and  $i$  for one set of intermediate winding parameters, and then used this relationship for all data generated from the simple model. As the pressure relationship from the full winding model assumes no air leakage, we can assume that the results of our simple model are self-consistent when the mass loss due to air flow is small. In cases where the mass loss is large, the full winding model is invalid for those specific conditions.

The numerical procedure is thus as follows. For the outer lap, the system (A3) is solved as written. When the next lap is added, the pressure load increases. The system (A3) is then solved again, where the initial condition (A3d) is replaced by the pressure field and height of the web at the end of the previous lap. This procedure is repeated as more laps are added to the roll.

**Air Loss Results.** We begin by obtaining the relationship between pressure loading,  $P_L$ , and the lap number,  $i$ , from the winding model; this relationship is used in the generation of all subsequent data from the simple air-leakage model. The winding model with air entrainment (no side leakage) was run to give the pressure loading and the lap number under the first lap (Fig. 17) using the winding conditions in test I of Table 1. We next proceeded to generate data from the simple air flow model following the algorithm in the preceding section. Note that as the full winding model is assumed to be isothermal, all subsequent calculations are for isothermal conditions, i.e.,  $\gamma=1$  in (A3) and (A4). Comparisons

between results for cases where the compressibility is assumed to be adiabatic versus isothermal show some relatively small quantitative differences, but the qualitative trends are the same. Figure 14 gives a plot of the percentage of the original air mass lost from the first lap of the roll as a function of the initial clearance between the web and the roll, for various web widths. Data is provided after winding 3089 laps for a winding speed of 2.54 m/s (500 ft/min); the air exits the web at the ambient atmospheric pressure. It is assumed that the initial pressure in the gap at time  $t=0$  is equal to the imposed load pressure (i.e.,  $\bar{P}_H=1$  in (A3) and (A4) in the first lap at the start of the calculation). Figure 15 provides data for the same conditions as Fig. 14, except at 7.62 m/s (1500 ft/min). Note that in generating these figures, we started our calculation when the 4th lap of the roll was added ( $P_H=0.105$  MPa and  $ca=h_0=1.464 \mu\text{m}$ ), as this is the first lap for which the pressure in the clearance (i.e., between the web and the roller) is larger than atmospheric pressure. In the simple model, if the pressure in the clearance is subatmospheric, then air moves into the gap and initially increases the clearance. Furthermore, the simple model predicts a relatively large increase in clearance; calculations show it takes hundreds of laps to again squeeze this increased mass out of the domain as the pressure loading increases. It is our opinion that this behavior is not physical, as the neglected local deformation of the web would presumably reduce this large increase in air mass. Figures 14 and 15 indicate that, as expected, wider webs with smaller initial clearances have smaller air leakage, where less air leakage occurs at faster winding speeds.

## References

- [1] Altmann, H. C., 1968, "Formulas for Computing the Stresses in Center Wound Rolls," *Tappi J.*, **51**, pp. 176–179.
- [2] Connolly, D., and Winarski, D. J., 1984, "Stress Analysis of Wound Magnetic Tape," *ASLE Special Publication SP-16*, pp. 148–157.
- [3] Hakiel, Z., 1987, "Nonlinear Model for Wound Roll Stresses," *Tappi J.*, **70**, pp. 113–117.
- [4] Qualls, W. R., 1995, "Hygrothermomechanical Characterization of Viscoelastic Centerwound Rolls," Ph.D. thesis, Oklahoma State University.
- [5] Good, J. K., Wu, Z., and Fikes, M. W. R., 1994, "The Internal Stresses in Wound Rolls With the Presence of a Nip Roller," *ASME J. Appl. Mech.*, **61**, pp. 182–185.
- [6] Good, J. K., and Holmberg, M. W., 1993, "The Effect of Air Entrainment in Centerwound Rolls," *Proceedings of the Second International Conference on Web Handling*, James K. Good, ed., Web Handling Research Center, Oklahoma State University, Stillwater, OK.
- [7] Good, J. K., and Covell, S. M., 1995, "Air Entrapment and Residual Stresses in Rolls Wound With a Rider Roll," *Proceedings of the Third International Conference on Web Handling*, James K. Good, ed., Web Handling Research Center, Oklahoma State University, Stillwater, OK.
- [8] Chang, Y. B., Chambers, F. W., and Shelton, J. J., 1996, "Elastohydrodynamic Lubrication of Air-Lubricated Rollers," *ASME J. Tribol.*, **118**, pp. 623–628.
- [9] Taylor, R. M., and Good, J. K., 1997, "Entrained Air Films in Center Wound Rolls—With and Without the Nip," *Proceedings of the Fourth International Conference on Web Handling*, James K. Good, ed., Web Handling Research Center, Oklahoma State University, Stillwater, OK.
- [10] Forrest, A. W., 1995, "Air Entrainment During Film Winding With Layon Rolls," *Proceedings of the Third International Conference on Web Handling*, James K. Good, ed., Web Handling Research Center, Oklahoma State University, Stillwater, OK.
- [11] Forrest, A. W., 1995, "Wound Roll Stress Analysis Including Air Entrainment and the Formation of Roll Defects," *Proceedings of the Third International Conference on Web Handling*, James K. Good, ed., Web Handling Research Center, Oklahoma State University, Stillwater, OK.
- [12] Bouquerel, F., and Bourgin, P., 1993, "Irreversible Reduction of Foil Tension Due to Aerodynamical Effects," *Proceedings of the Second International Conference on Web Handling*, James K. Good, ed., Web Handling Research Center, Oklahoma State University, Stillwater, OK.
- [13] Bourgin, P., 1997, "Air Entrainment in Web Handling: To be Avoided or Mastered?" *Proceedings of the Fourth International Conference on Web Handling*, James K. Good, ed., Web Handling Research Center, Oklahoma State University, James K. Good, ed., Web Handling Research Center, Oklahoma State University, Stillwater, OK.
- [14] Forrest, A. W., 1999, "Optimization of Equipment and Process Conditions for Film Winding," *Proceedings of the Fifth International Conference on Web Handling*, James K. Good, ed., Web Handling Research Center, Oklahoma State University, Stillwater, OK.

- [15] Pfeiffer, J. D., 1981, "Measurement of K2 Factor for Paper," *Tappi J.*, **64**, pp. 105–106.
- [16] Pfeiffer, J. D., 1999, "Compressive Modulus Measurement Techniques," *Proceedings of the Fifth International Conference on Web Handling*, James K. Good, ed., Web Handling Research Center, Oklahoma State University, Stillwater, OK.
- [17] Forrest, A. W., 1993, "A Mathematical and Experimental Investigation of the Stack Compression of Films," *Proceedings of the Second International Conference on Web Handling*, James K. Good, ed., Web Handling Research Center, Oklahoma State University, Stillwater, OK.
- [18] Rice, B. S., Cole, K. A., and Müftü, S., 1999, "An Experimental and Theoretical Study of Web Traction Over a Nonvented Roller," *Proceedings of the Fifth International Conference on Web Handling*, James K. Good, ed., Web Handling Research Center, Oklahoma State University, Stillwater, OK.
- [19] Timoshenko, S., 1970, *Theory of Elasticity*, McGraw-Hill, New York, p. 418.